Scripta Materialia 147 (2018) 88–92

Contents lists available at ScienceDirect

Scripta Materialia

journal homepage: www.elsevier.com/locate/scriptamat

Regular article

Recovery of tensile properties of twinning-induced plasticity steel via electropulsing induced void healing

C.L. Yang [a,b], H.J. Yang [a,*], Z.J. Zhang [a], Z.F. Zhang [a,b,**]

[a] Shenyang National Laboratory for Materials Science, Institute of Metal Research, Chinese Academy of Sciences, 72 Wenhua Road, Shenyang 110016, PR China
[b] University of Chinese Academy of Sciences, 19 Yuquan Road, Beijing 100049, PR China

ARTICLE INFO

Article history:
Received 30 November 2017
Received in revised form 6 January 2018
Accepted 8 January 2018

Keywords:
TWIP steel
Electropulsing
Void healing
Recovery
Strength and plasticity

ABSTRACT

The effects of electropulsing treatment (EPT) and annealing on the tensile behaviors of twinning-induced plasticity (TWIP) steel after interrupted tension are compared. It is found that EPT effectively restores the tensile property of specimens with macro voids completely, while annealing could not. The selective heating and thermal compressive stress induced by EPT around voids make them readily to be healed while keeping the matrix unchanged. The healing effect of voids improves the strain-hardening capability of TWIP steels and leads to the recovery of strength and elongation of the EPT specimen, relative to those annealed counterparts.

Twinning-induced plasticity (TWIP) steel exhibits an outstanding combination of tensile strength and uniform elongation [1–3], making it a potential structural material for auto and aerospace industry [4]. Previous studies [5, 6] have shown that the high strength and ductility of TWIP steels can be attributed to the high strain-hardening capacity, which is caused by deformation twinning [7–9]. Whereas, microvoids always initiate in TWIP steels during plastic deformation [10, 11], which will weaken the strain-hardening capability of TWIP steels and lead to the premature initiation of necking [12]. Therefore, the mechanical properties of TWIP steels are severely harmed by the existence of macro voids [13–15].

Fortunately, plenty of studies [16–18] have reported that cracks in steels can be effectively healed by electropulsing treatment (EPT). The crack-healing effect of EPT may be attributed to two aspects [19]: 1) the elevated temperature near the crack and 2) the thermal compressive stress around the crack. The thermal effect near a crack is much larger than that far away from the crack during EPT. A previous study [20] has shown that the temperature rise near a crack can be 3–4 times higher than that of the whole specimen during EPT, that is, the materials near a crack might be molten while the whole specimen stays solid. Furthermore, the compressive stress around a crack is caused by the high temperature near the crack [21]. The materials around a crack will expand as the temperature around the crack increases, whereas the material far away from the crack will not expand that much. Thus, the outwards expanding of the materials around a crack may be restricted by the surrounding materials and then the melted metal is compressed into the crack. Therefore, cracks might be healed after cooling. Similar to the crack-healing effect of EPT, the healing of the macro voids through EPT can also be expected, which will effectively improve the mechanical properties of TWIP steels. Besides, another advantage of EPT is that its duration is very short with an order of ~0.1 ms, which ensures its efficiency in industrial applications.

Previous studies have reported the effect of EPT on the mechanical behavior of boron steel [24] dual-phase steel [25] and stainless steel [26]. This study presents the effect of EPT on the mechanical behavior of TWIP steel with macro voids, comparing with the effect of annealing. It is interesting to find that both the strength and plasticity of the TWIP steels with defects were synchronously recovered by EPT, while those of the annealed ones did not.

High-Mn TWIP steels with the composition of Fe-22Mn-0.9C produced by induction furnace melting were used in this study. The cast ingot was kept at 1000 °C for 2 h, and then immediately hot forged to square rod with a final dimension of 25 × 25 mm^2 at 800–1000 °C. After that, the rod was subjected to solution annealing at 1050 °C for 1 h followed by water quenching. The specimens for tensile tests were sparking cut along the axial direction with gauge sectional dimensions of 15 × 4 × 3 mm^3. Before tensile tests, all the specimens were electropolished in a mixed solution of perchloric acid and glacial acetic acid with a ratio of 1:9 for 1 min at 15 °C and 12 V, in order to produce a strain-free and smooth surface. Tensile tests were carried out at a strain rate of 10^{-3} s^{-1} by an INSTRON 5982 testing machine at room

* Corresponding author.
** Corresponding author at: University of Chinese Academy of Sciences, 19 Yuquan Road, Beijing 100049, PR China.
E-mail addresses: hjyang@imr.ac.cn (H.J. Yang), zhfzhang@imr.ac.cn (Z.F. Zhang).

https://doi.org/10.1016/j.scriptamat.2018.01.008
1359-6462/

temperature and the strain was measured with an extensometer. For each case three samples were tested to ensure the repeatability and credibility of the results. Interrupted tensile tests at a true strain of ~37.5% were carried out with four identical TWIP steel specimens, marked as #1, #2, #3 and #4, respectively, in order to introduce macro voids into these specimens [12]. After beforehand tension, the four TWIP steel specimens experienced different treatments that will be described below. Final tensile tests were conducted with the four TWIP specimens after different treatments.

After the beforehand tension, the #2 specimen was annealed at 500 °C for 10 min, #3 was annealed at 1000 °C for 10 min and #4 was electropulsing treated and #1 specimen did not experience any treatment. The annealing was conducted under the protection of argon environment. EPT was carried out by a self-made equipment with a capacitor bank discharge circuit at ambient temperature. The experimental discharge voltage was chosen 3 kV and the current pulse duration was 400 ns. The specimen was connected to two copper electrodes during EPT. Then the #4 specimen was cooled at room temperature.

In order to characterize the microstructure of the specimens after beforehand tension and various treatments, another four Fe-22Mn-0.9C TWIP steel samples were prepared following the same treatments conducted with the above four tensile specimens. The microstructures of the samples after different treatments were characterized by a LEO Supra 35 field emission scanning electron microscopy (SEM) equipped with an electron backscattered diffraction (EBSD) detector and an FEI Tecnai F20 transmission electron microscopy (TEM). Furthermore, a Versa XRM-500 three-dimensional X-ray tomography (3D-XRT) was used to detect the macro voids before and after EPT.

Fig. 1 shows the results of the tensile tests conducted with the Fe-22Mn-0.9C TWIP steel specimens. The stress-strain curves of the four identical TWIP steel specimens strained to a true strain of ~37.5% are exhibited in Fig. 1(a), which strongly suggests that the tensile behaviors of the four TWIP steel specimens are congruent with each other. Almost the identical microstructures, thus, can be expected in the four TWIP steel specimens. It should be mentioned that macro voids can be introduced to the TWIP steel specimens after beforehand tension according to the previous study [12] which demonstrates that some macro voids can be detected in the Fe-22Mn-0.9C TWIP steel specimens strained to 25%. Fig. 1(b) shows the final stress–strain curves of the four Fe-22Mn-0.9C TWIP steel specimens after different treatments. The yielding strengths (YS) of the four specimens decrease ~400 MPa, ~800 MPa and ~700 MPa after 550 °C annealing, EPT and 1000 °C annealing, respectively. That is, the YS of the electropulsing treated specimen sets between those of the 550 °C and 1000 °C annealed specimens. For the annealed specimens, the ultimate tensile strength (UTS) and uniform elongation (UE) exhibit a trade-off relationship, i.e. as the UTS decreases, the UE increases. Whereas, the UTS and UE of the electropulsing treated specimen break this trade-off relationship. That is, the UTS and UE of the electropulsing treated specimen were improved synchronously compared to the annealed counterparts. The stress–strain curves of the #1 specimen (without any treatment) and #4 specimen (after EPT) are presented in Fig. 1(c), where the joint of the two stress–strain curves (red and black) of #1 specimen illustrates the tensile stress–strain behavior of the initial Fe-22Mn-0.9C TWIP steel specimen before the interrupted tension. It is indicated that the tensile properties, such as YS, UTS and UE, of the electropulsing treated specimen are in line with those of the initial void-free specimen. That is to say, the EPT may remove the influence of the macro voids after the beforehand tension, which will be further discussed below.

In order to understand the different effects of annealing and EPT on the microstructure of TWIP steels, SEM and TEM observations were conducted. Fig. 2 shows the EBSD and TEM images of four Fe-22Mn-0.9C TWIP steel samples experienced the same beforehand tension and various treatments as mentioned above. Fig. 2(a) and (b) are the EBSD and TEM images of #1 specimen which was strained to a true strain of ~37.5% without any further treatment. As shown in Fig. 2(a), the grain size of #1 specimen after beforehand tension is ~20 μm and the orientation of grains distribute uniformly. Besides, large amounts of deformation twins and second twins spread uniformly in #1 specimen and the thickness of the deformation twins is ~10 nm as exhibited in Fig. 2(b) with the selected area electron diffraction (SAED) pattern inserted. Fig. 2(c) and (d)are the EBSD and TEM images of #2 specimen which is strained to a true strain of ~37.5% followed by annealing at 550 °C. After annealing, deformation twins disappear and a few annealing twins can be observed. Besides, the average grain size of the #2 specimen reduced to ~5 μm, which may be mainly due to recrystallization. Fig. 2(d) presents the configuration of annealing twins and corresponding SAED pattern. Fig. 2(e) and (f) are the EBSD and TEM images of the #3 specimen which is strained to a true strain of ~37.5% followed by annealing at 1000 °C. The grain size of the #3 specimen increases obviously to ~50 μm and the distribution of grain orientation is also uniform, as shown in Fig. 2(e). Meanwhile, abundant annealing twins can be observed and the thickness of the annealing twins is ~100 nm, as exhibited in Fig. 2(f). Fig. 2(g) and (h) are the EBSD and TEM images of the #4 specimen which is strained to a true strain of ~37.5% followed by EPT. Both large grains and small grains can be observed, which may be formed by grain growth and recrystallization, respectively. Besides, different from the thick annealing twins observed in the annealed specimens, thin twins can be observed in the #4 specimen after EPT, as exhibited in Fig. 2(h). These thin twins should be formed by the beforehand tension, that is, deformation twins can be retained during EPT. As is well known, twin boundary is a coherent boundary with relatively lower electric resistance and then the temperature rise around twin boundaries during EPT should be small. Therefore, EPT seems to more like a selective annealing method: heating the parts with higher electric resistance, while retaining the parts with lower electric resistance. This selective annealing effect of EPT is of great significance in industrial applications: it maintains the microstructure and then the mechanical properties of the matrix while repairs damages.

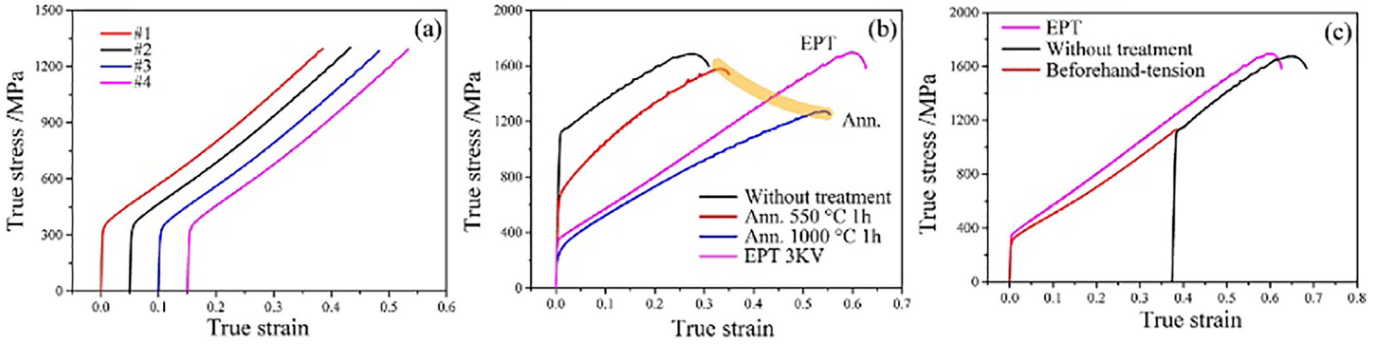

Fig. 1. (a) The beforehand tensile curves of four identical Fe-22Mn-0.9C TWIP steel specimens with a true strain of ~37.5%, (b) The final tensile curves of the four TWIP steel specimens and (c) compare the tensile behaviors of the electropulsing treated specimen to the initial specimen.

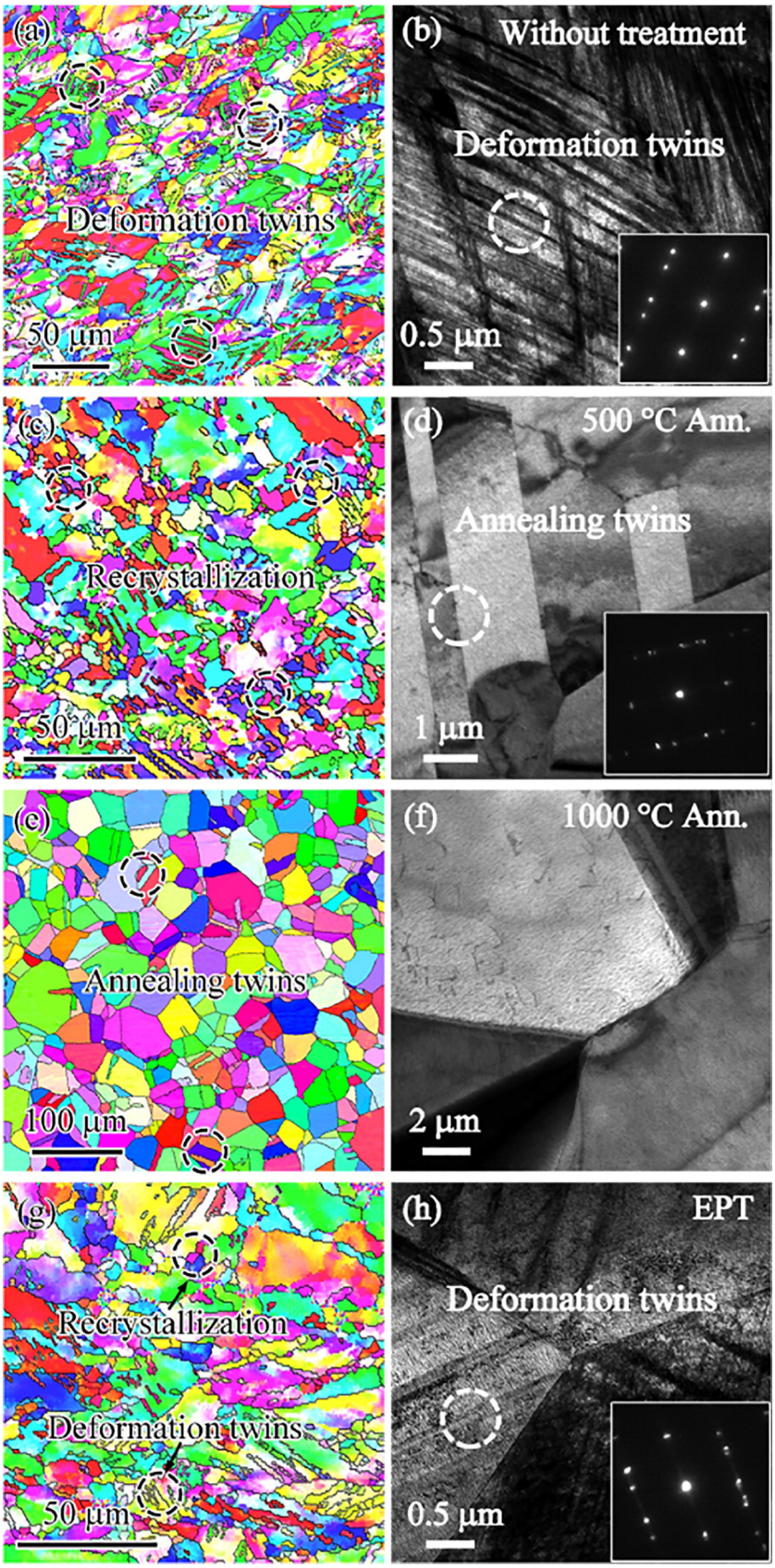

Fig. 2. The EBSD and TEM images of the four TWIP steel specimens after corresponding treatment: (a) and (b) large amounts of deformation twins in the specimen after beforehand tension, (c) and (d) partly recrystallized microstructure of the specimen after annealed at 500 °C, (e) and (f) fully recrystallized microstructure of the specimen after annealed at 1000 °C, (g) and (h) restored microstructure of the specimen after EPT.

In addition to the selective annealing effect, EPT may also repair the macro voids in the TWIP steel specimens formed during beforehand tension, which can be attributed to the temperature rise and compressive stress associated with EPT. The temperature rise of the material during EPT depends on the energy input by the electropulsing, which can be written as [19]:

$$\Delta T = \frac{j^2 \rho t}{c_p d}, \tag{1}$$

where j is the electric current density during electropulsing time t, ρ is the electrical resistivity of the material, c_p is the specific heat and d is the density of the specimen. Whereas, the temperature rise is not homogenous in the specimen during EPT: j varies for different sites. The electric current j near a crack can be described as [20]:

$$j = j_0 \cdot f(x, y, a, b), \tag{2}$$

where j_0 is the amplitude of the electric current density far from the crack and $f(x, y, a, b)$ is a function of the location relative to the crack and the length of the major and minor axis of the crack. Qin et al. [20] calculated the temperature rise near a crack tip (with the major axis of ~10 μm and the minor axis of ~1 μm) under the average current density of ~10 A/cm^2. The result shows that the temperature rise near the crack tip is about 4 times higher than that of the site far away from the crack. Therefore, based on the above discussion, the temperature rise near a crack is much higher than that of the matrix. This increment in the temperature serves to melt the material near defects. Meanwhile, due to the non-synchronous temperature increment and thermal expansion, a compressive stress may occur around a crack, which can be written as [19]:

$$\Delta\sigma = E\alpha \cdot \Delta T, \tag{3}$$

where E is the Young's modulus of the material, α is the thermal expansion coefficient. This compressive stress serves to push the molten materials into the crack and then the crack is repaired after solidification.

Fig. 3 presents the quasi in-situ observations of the TWIP steel samples before (a), (c), (e) and after (b), (d), (f) EPT. As can be seen from SEM images in Fig. 3(a) and (b), the initial surface macro voids with diameters about 2 μm become smaller and even disappear after EPT, indicating a clear healing effect. Apart from the macro voids, some inclusions in the specimens, at which macro voids usually initiate, are also removed after EPT as shown in Fig. 3(c) and (d). Therefore, the effect of EPT on TWIP steels does not only heal macro voids but also prevent void initiation in the later tension.

Aside from the above evidence on the sample surface, the healing effect of EPT can also be verified by XRT from the inside of the sample. The internal damages of metals can be directly characterized by XRT and then any possible pseudomorph introduced during the quasi in-situ processing is prevented. Fig. 3(e) and (f) show the XRT images of a crack in a strained TWIP steel specimen before and after EPT, respectively. It is obvious that the crack with a length of ~400 μm is separated into several short cracks, as indicated by the dotted circles in Figs. 3(e) and (f). The total length of the crack has been reduced to ~300 μm after EPT. In addition, the size of the void at the bottom of Fig. 3(e) has also been refined significantly after EPT, which is shown in Fig. 3(f).

Therefore, based on the quasi in-situ SEM and XRT observations, it is confirmed that there is an obvious void-healing effect in the TWIP steel after EPT. For some engineering components under cyclic deformation, microcracks usually initiate inside and reduce their lifetime [22, 23]. Thus, EPT may be used as a healing or repairing method for these engineering alloys with damages to improve the serving time.

Based on the above observation, the synchronous improvement of the UTS and UE of the electropulsing treated TWIP steel specimens, relative to those of the annealed one, can be attributed to the void-healing effect. According to the previous study, the influence of macro voids on Θ can be written as [12]:

$$\Theta_{void} = \frac{d\sigma}{d\varepsilon} - \frac{d\dfrac{\sigma}{1-A_v}}{d\varepsilon}, \tag{4}$$

where $\frac{d\sigma}{d\varepsilon} = \Theta$ can be obtained from the stress-strain curve and A_v is the cross-sectional area of voids. After fitting the experimental data of A_v, the Θ_{void} can be calculated and it increases exponentially as strain increases [12]. That is, the evolution of macro voids severely reduces the strain-hardening capability of TWIP steels at large strains. Therefore, the void-healing effect of EPT postpones the evolution of macro voids and then the strain-hardening capability of electropulsing treated specimen is improved, as shown in Fig. 4. According to the Considère criterion, necking happens when the applied stress reaches the strain-hardening rate. Thus, improving the strain-hardening capability

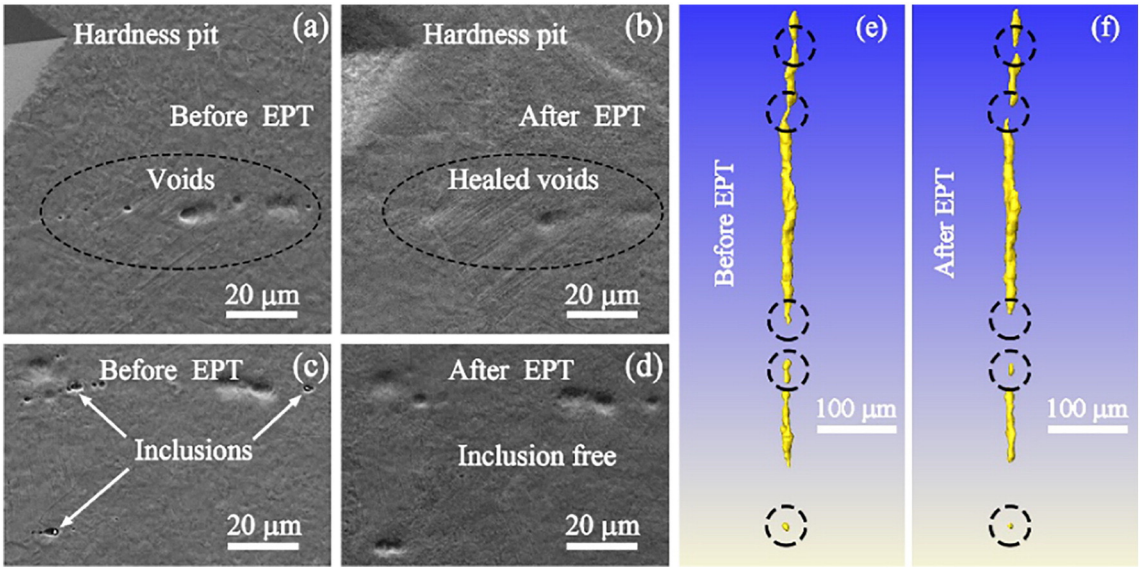

Fig. 3. Quasi in-situ observations of the defective samples conducted with EPT by SEM (a-d) and XRT (e–f) techniques: the void-healing effect (a–b), the elimination of inclusions (c–d) and the crack-healing effect inside the specimen (e–f).

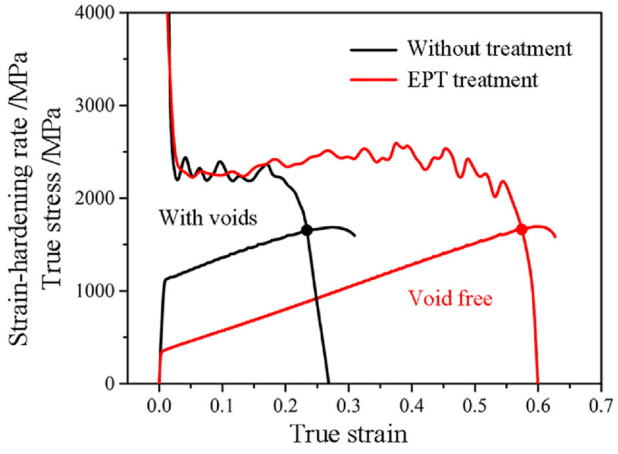

Fig. 4. Comparison of the strain-hardening behaviors of the TWIP steel with and without macrovoids, showing the improvement of the strain-hardening capability of TWIP steel specimens by healing the macrovoids and removing the inclusions.

postpones the initiation of necking and further results in the synchronously enhanced UTS and UE.

To be specific, based on Fig. 3(e), the cracks with a width less than ~5 μm can be completely healed by EPT with a discharge voltage of 3 kV. Meanwhile, according to the previous study [12], the average radius of the voids in the Fe-22Mn-0.9C TWIP steel specimens strained to 45% is ~2 μm. Thus, the average size of the macro voids in the current specimens after beforehand tension should be smaller than 2 μm due to smaller plastic strain applied. That is, the macro voids formed by the beforehand tension can be completely healed after the EPT with a discharge voltage of 3 kV. Therefore, the microstructure of the electropulsing treated specimen completely restored to the initial state before tension, which is verified by the similarity between the tensile curves of the electropulsing treated specimen and the jointed one as shown in Fig. 1(c). Meanwhile, the inclusions in TWIP steel specimens are also removed, which impedes void initiation during later tension. On the contrary, annealing does not have this healing effect. The temperature in the specimen during annealing is basically homogenous, which is not high enough to melt the materials around crack tip or remove the inclusions. Thus, the macro voids caused by the beforehand tension still exist in the specimens after annealing. The existence of macro voids severely reduces the strain-hardening capability of TWIP steel specimens, which leads to an early initiation of necking, as shown in Fig. 4. Therefore, both the UTS and UE of the electropulsing treated TWIP steel specimen are higher than those of the annealed one.

To sum up, by compared with annealing, EPT recovered the tensile properties, such as UTS and UE, of TWIP steels with macro voids, which can be attributed to its damage-healing effect. EPT does not only heal existent macro voids but also remove the inclusions in TWIP steel specimens, which impedes void evolution in the future plastic deformation. Meanwhile, the matrix grains without macro voids mainly keep stable during EPT due to lower temperature rise relative to that of the sites with macro voids. This healing effect may significantly improve the strain-hardening capability of TWIP steel specimens, which postpones the initiation of necking and then improves the UTS and UE simultaneously.

Acknowledgements

Financial supports from the National Natural Science Foundation of China (Grant Nos. 51501196, and 51331007) and IMR foundation for "Young merit scholars" and Youth Innovation Promotion Association CAS, No. 2017235, are gratefully acknowledged.

References

[1] J.K. Kim, L. Chen, H.S. Kim, S.K. Kim, Y. Estrin, B.C. De Cooman, Metall. Mater. Trans. A Acta Mater. 40A (2009) 3147–3158.
[2] J. Lin, X. Wang, W. Ren, X. Yang, Q. Wang, J. Mater. Sci. Technol. 32 (2016) 783–789.
[3] B. Fu, L. Fu, S. Liu, H.R. Wang, W. Wang, A. Shan, J. Mater. Sci. Technol. (2017) https://doi.org/10.1016/j.jmst.2017.09.017.
[4] L. Chen, Y. Zhao, X. Qin, Acta Metall. Sin. Engl. Lett. 26 (2013) 1–15.
[5] A. Bintu, G. Vincze, C.R. Picu, A.B. Lopes, J.J. Gracio, F. Barlat, Mater. Sci. Eng. A 629 (2015) 54–59.
[6] H. Idrissi, K. Renard, L. Ryelandt, D. Schryvers, P.J. Jacques, Acta Mater. 58 (2010) 2464–2476.
[7] I.U. Gutierrez, D. Raabe, Acta Mater. 59 (2011) 6449–6462.
[8] K. Renard, H. Idrissi, D. Schryvers, P.J. Jacques, Steel Res. Int. 83 (2012) 385–390.
[9] K. Renard, P.J. Jacques, Mater. Sci. Eng. A 542 (2012) 8–14.
[10] D. Fabregue, C. Landron, O. Bouaziz, E. Maire, Mater. Sci. Eng. A 579 (2013) 92–98.
[11] C. Landron, O. Bouaziz, E. Maire, J. Adrien, Scr. Mater. 63 (2010) 973–976.
[12] C.L. Yang, Z.J. Zhang, P. Zhang, Z.F. Zhang, Acta Mater. 136 (2017) 1–10.
[13] T. Lee, M. Koyama, K. Tsuzaki, Y.H. Lee, C.S. Lee, Mater. Lett. 75 (2012) 169–171.
[14] X. Peng, D.Y. Zhu, Z.M. Hu, W.F. Yi, H.J. Liu, M.J. Wang, Mater. Des. 45 (2013) 518–523.
[15] M. Koyama, T. Lee, C.S. Lee, K. Tsuzaki, Mater. Des. 49 (2013) 234–241.
[16] A. Hosoi, T. Nagahama, Y. Ju, Mater. Sci. Eng. A 533 (2012) 38–42.
[17] H. Song, Z.-J. Wang, Mater. Sci. Eng. A 490 (2008) 1–6.
[18] Y.Z. Zhou, J.D. Guo, M. Gao, G.H. He, Mater. Lett. 58 (2004) 1732–1736.
[19] W. Zhang, M.L. Sui, Y.Z. Zhou, D.X. Li, Micron 34 (2003) 189–198.
[20] R.S. Qin, S.X. Su, J. Mater. Res. 17 (2002) 2048–2052.
[21] J.D. Guo, X.L. Wang, W.B. Dai, Mater. Sci. Technol. 31 (2015) 1545–1554.
[22] Y. Ogawa, D. Birenis, H. Matsunaga, A. Thogersen, O. Prytz, O. Takakuwa, J. Yamabe, Scr. Mater. 140 (2017) 13–17.
[23] T. Leitner, S. Pillmeier, K.S. Kormout, R. Pippan, A. Hohenwarter, Scr. Mater. 139 (2017) 39–43.
[24] B.D. Ma, Y.G. Zhao, J. Ma, H.C. Guo, Q. Yang, J. Alloys Compd. 549 (2013) 77–81.
[25] W.J. Lu, R.S. Qin, Mater. Sci. Eng. A 677 (2016) 252–258.
[26] Y.R. Ma, H.J. Yang, Y.Z. Tian, J.C. Pang, Z.F. Zhang, Mater. Sci. Eng. A 713 (2018) 146–150.